Probing Gardner Physics in an Active Quasithermal Pressure-Controlled Granular System of Noncircular Particles

Hongyi Xiao⊙, Andrea J. Liu⊙, and Douglas J. Durian⊙*

Department of Physics and Astronomy, University of Pennsylvania, Philadelphia 19104, Pennsylvania, USA

To search for experimental signals of the Gardner crossover, an active quasithermal granular glass is constructed using a monolayer of air-fluidized star-shaped particles. The pressure of the system is controlled by adjusting the tension exerted on an enclosing boundary. Velocity distributions of the internal particles and the scaling of the pressure, density, effective temperature, and relaxation time are examined, demonstrating that the system has key features of a thermal system. Using a pressure-based quenching protocol that brings the system into deeper glassy states, signals of the Gardner crossover are detected via cage size and separation order parameters for both particle positions and orientations, offering experimental evidence of Gardner physics for a system of anisotropic quasithermal particles in a low spatial dimension.

Glasses made of atoms, polymers, colloids, or grains constitute an important class of materials, yet the understanding of their physics is far from complete [1,2]. In some cases, a Gardner transition is predicted as a system is quenched into deeper glassy states by lowering temperature or increasing density [3,4]. At such a transition, metastable basins in the energy landscape break up into a hierarchy of sub-basins, leading to a marginal glass phase that affects all physical properties of a glass, including linear and non-linear mechanical response and low-temperature behavior [5–7]. While the theoretical framework has been established for spin glasses and structural glasses of high spatial dimension [3,8–13], and has been studied extensively in low-dimensional simulations [7,14–23], there have been relatively few experiments [24–28]. Moreover, computational studies, as well as all the experiments showing direct evidence of Gardner physics by following particle tracks, have been restricted to systems with isotropic (spherically symmetric) interactions, yet nearly all real-world glasses have constituent particles of complex shapes, with both translational and rotational degrees of freedom.

Scalliet *et al.* have shown that the existence of Gardner physics depends on the form of particle interactions in systems with spherically symmetric potentials [16,20]. This raises the question of whether we might expect to find Gardner physics in systems with nonisotropic interactions. Two experiments have searched for Gardner signatures indirectly in molecular glass formers: dielectric response measurements of sorbitol and xylitol exhibited broadening of intermediate relaxation consistent with a Gardner transition [25], while nonlinear susceptibility measurements in glycerol [27] failed to find signs of Gardner physics. To fill this gap, we present the first direct evidence for Gardner physics in a 2D system with nonisotropic interactions, and

show that not only particle translations but also their orientational degrees of freedom provide consistent indicators of Gardner physics. While the existence of a sharp Gardner transition in 3D is still debated [22,29], in 2D systems such as ours, long-ranged fluctuations are expected to reduce the transition to a sharp crossover [19].

Our experimental system consists of a monolayer of air-fluidized particles under controlled pressure. Three major differences exist in comparison to previous works. First, the particles are star-shaped with five spokes (Fig. 1), which not only breaks interaction isotropy but prevents crystallization. The concavity of the particles enhances caging at a
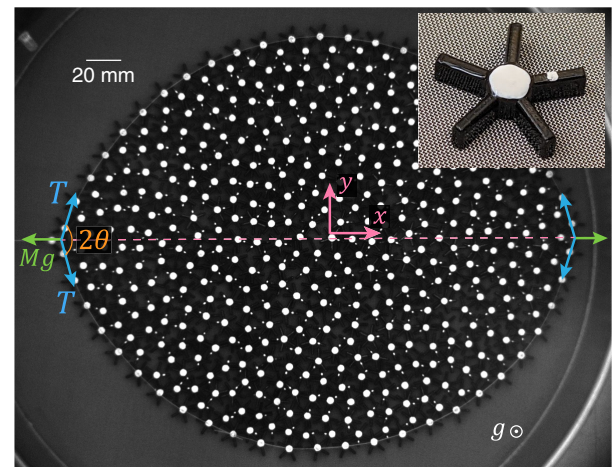

FIG. 1. Photograph of the pressure-controlled experiment with star-shaped particles (inset). Air-fluidized particles are enclosed by a boundary made of a chain of particles on a thin flexible thread. The left end is pulled with a controlled force $G = Mg$, while the right end is anchored. See the Supplemental Material [34] for an example video.

248001-1

lower density, which suppress localized cage-breaking events that can impair Gardner physics. Second, air fluidization injects energy with spatial and temporal uniformity by a sublevitating upflow of air that sheds turbulent wakes to induce in-plane stochastic particle motion [30,31]. Injecting energy at the particle scale renders the system an active matter and leads to behaviors with a strong thermal analogy [31–33]. Unlike vibration-based approaches, air fluidization does not generate large convection currents of particles. As the particle weight is largely countered by the air pressure, the basal friction with the substrate becomes small. Third, a pressure-controlled protocol is implemented, which previously has only been realized computationally [18,19]. This is important because in systems of hard particles, the pressure depends extremely sensitively on density in the Gardner regime. And the range between the Gardner crossover and jamming is considerably narrower in terms of density [24] than pressure. Pressure can be more accurately controlled than density for finite numbers of particles for locating the Gardner crossover.

Experimental details are as follow: The particles have five evenly spaced spokes of length 4.5 mm, width 1.25 mm, and height 2.5 mm, surrounding a 4 mm diameter circular disk. The nominal particle diameter is thus $\sigma = 13.0$ mm. The particles are 3D-printed with the Polyjet technique using a black rigid resin with mass density 1.18 g/cm³. The particles have mass $m = 0.12$ g and moment of inertia $I = 1.73$ g/mm². The fluidization apparatus is based on a previous device [31–33,35], where the particles are placed on a sieve with 150 μm mesh size. The air velocity is set to 3.6 m/s to minimize particle-substrate sliding friction without levitating the particles.

As shown in Fig. 1, the particles are enclosed by a flexible boundary of 50 particles glued to a thin flexible string with center-to-center spacing of 14 mm. These boundary particles are also fluidized, resulting in better uniformity of particle behaviors compared to rigid boundaries. The right end of the boundary is fixed while the left end is pulled by a constant force, $G = Mg$, where M is the mass of a hanging weight and $g = 9.8$ m/s². This results in a force balance of $G = 2T \cos \theta$ at the ends with T being the string's tension and θ being the half angle made by the string. For the rest of the boundary, a Laplace-like relation can be established for the particle pressure, $P = T/R$, with $1/R$ being the boundary curvature. The shape of the upper and lower halves of the boundary can be well fitted to a circular arc, indicating a constant R. Thus, the pressure of the system is controlled by the hanging mass via $P = G/2R \cos \theta$.

Two series of experiments were performed. First, to study the thermal analogy and explore phase space, the system is held at a constant pressure using various hanging weights G and numbers N of interior particles. In each case, the system is equilibrated at the desired G for 10 min, after which 1 min of data were taken. Second, to probe the
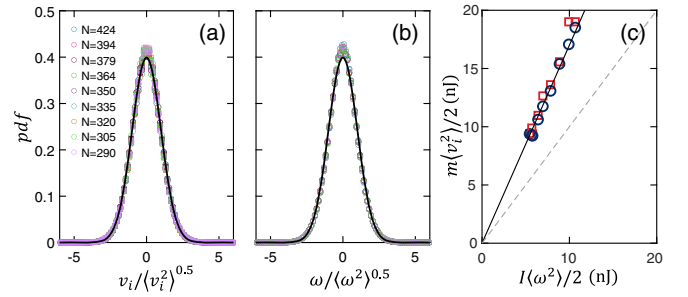

FIG. 2. Distributions of (a) the normalized translational speeds, v_i, with $i = x$, y and (b) the angular velocity, ω, for internal particles from cases with different number of particles, N, under a constant hanging weight of $G = 0.58 \times 10^{-3}$ N. The black curves are the standard Gaussian distribution. (c) The translational energies $m\langle v_i^2 \rangle/2$ (red square for $i = x$, blue circle for $i = y$) vs the average rotational energy $I\langle \omega^2 \rangle/2$. The solid line is a linear fit with a slope of 1.7.

Gardner physics, a pressure-based quenching protocol was developed (below). Digital videos were recorded at 110 fps for the first set of experiments and at 12 fps for the quenching experiments, with 50 pixels/σ resolution. The center and one spoke of each particle were painted white to enable particle tracking [36] with uncertainty of 0.004σ for position and 0.014 rad for orientation. Internal particles that are at least 3σ away from the boundary are tracked for analysis, while boundary particles are used for calculating θ, R, and the packing density ϕ. A dynamical coordinate system is adopted with the x direction aligned with the end-to-end vector.

At low density and pressure, the behavior is analogous to a liquid in thermal equilibrium based on the distributions of translational and rotational velocities, shown in Figs. 2(a) and 2(b) for cases with varying N. After normalizing the velocities by their root mean square value, all the data collapse to the standard Gaussian distribution, indicating thermal behavior. The end-to-end distance fluctuates around a constant value, indicating mechanical equilibrium. Figure 2(c) examines the energy partition, showing that the two translational degrees of freedom have the same energy, $m\langle v_i^2 \rangle/2$, which is somewhat larger than the rotational energy, $I\langle \omega^2 \rangle/2$. The difference between the rotational and translational kinetic energies indicates that this active system is not perfectly thermal. In another set of such experiments, conducted with $N = 454$ and higher G ranging from 0.58×10^{-3} N to 9.11×10^{-3} N, the system experiences a glass transition with the relaxation time greatly increasing; here, quasithermal equilibrium cannot be reached within a reasonable wait time.

As a check we performed auxiliary experiments by enclosing the particles in a rectangular box and tilting the apparatus by an angle of β [33,37] [inset of Fig. 3(a)]. In this way, the local hydrostatic pressure is determined by the depth, $P = N_a(h)mg \sin \beta/W$, where $N_a(h)$ is the number
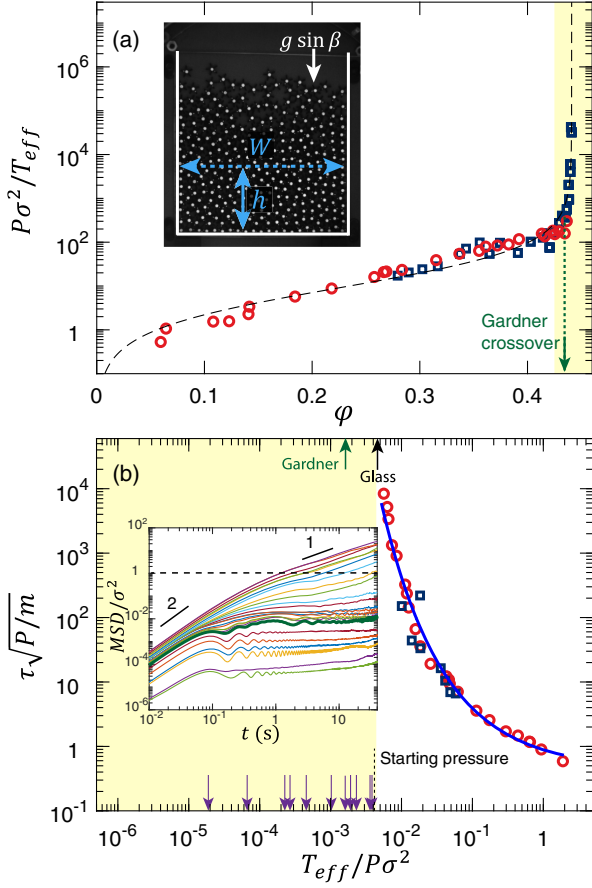
FIG. 3. State parameters for the granular system: (a) Dimensionless pressure vs density for the pressure controlled (blue square) and inclined (red circle) experiments, with fitted equation of state (dashed curve). Inset shows the inclined experiment. (b) Dimensionless relaxation time vs dimensionless effective temperature for cases with measurable relaxation times. The blue curve represents a fit to $y = a \exp(b/x^c)$ with $a = 0.45$, $b = 0.69$, and $c = 1/2$. Inset shows the MSD for the pressure-controlled experiments, with the thick green curve being the MSD at the Gardner crossover. The shaded region marks the glass phase and the arrows represent the $T_{\mathrm{eff}}/P\sigma^2$ of cases for testing the Gardner physics, with the corresponding density ranging from $\phi = 0.429$ to $\phi = 0.441$.

of particles above a distance h and W is the width of the box. The corresponding local packing density, ϕ, is extracted via binning. Several data points at different depths can be extracted from a single experiment, and various cases with varying β and numbers of particles were tested.

Figure 3(a) examines the equation of state for the system using pressure, packing density, and an effective temperature defined from the translational energy of the particles, $T_{\mathrm{eff}} = (1/2)m\langle v_x^2 + v_y^2 \rangle$. The dimensionless pressure, $P\sigma^2/T_{\mathrm{eff}}$, is plotted versus ϕ for both the pressure-controlled and the inclined experiments, showing a good agreement and thus validating our pressure-control scheme. An equation of state based on a Free Volume

Theory [33,37,38] is fitted to the data, $P\sigma^2/T_{\mathrm{eff}} \propto \phi/[1 - (\phi/\phi_c)^{1/2}]$, where $\phi_c = 0.441$ is approximately the point at which the pressure diverges and the jamming transition occurs. Note that ϕ_c is about half that for circular disks. The fitted equation of state describes the data well for the system both in "equilibrium" (corresponding to the experiments shown in Fig. 2) and out of equilibrium [33], reinforcing the strength of the thermal analogy.

At ϕ close to ϕ_c, the pressure increases drastically, indicating a glass phase. To identify the region of interest for exploring Gardner physics, the relaxation time, τ, is measured by the time for the mean-squared displacement (MSD) of the particles to reach 1 σ^2. Figure 3(b) shows the dimensionless relaxation time, $\tau\sqrt{P/m}$, vs the dimensionless effective temperature $T_{\mathrm{eff}}/P\sigma^2$. The results can be well fitted to a stretched exponential [33] of form $\tau\sqrt{P/m} = a \exp[b/(T_{\mathrm{eff}}/P\sigma^2)^c]$. As $T_{\mathrm{eff}}/P\sigma^2$ decreases, the relaxation time increases rapidly and the MSD curve develops a plateau due to caging (Fig. 3(b) inset). Per convention, we define the system to be in the glass phase when its inherent structure does not relax in $\tau_g = 24$ h. Additional long-duration experiments were performed to determine the glass transition point, $P_g = 0.012$ N/m, $\phi_g = 0.425$, and $\tau_g\sqrt{P_g/m} = 8.6 \times 10^5$, which corresponds to the experimental configuration with $N = 454$, and $G = 1.36 \times 10^{-3}$ N. Deep in the glass phase at even lower $T_{\mathrm{eff}}/P\sigma^2$, the MSD slowly increases after the initial plateau, which agrees with previous numerical simulations of hard spheres in the Gardner phase [15,18].

To probe the Gardner crossover quantitatively, we employ a quenching protocol in the glass phase (shaded region in Fig. 3) with a far wider pressure range than density range. We start with $G_0 = 1.55 \times 10^{-3}$ N and quench the system to higher pressures in discrete steps. For each step, the weight is held at G_0 initially for 100 s, then switched to a higher weight, G_{high}, and held for another 100 s for the system to approximately reach a mechanical equilibrium, setting the quenching pressure, p_{high}. This repeated-quench protocol is accomplished by tying two weights along the hanging string at different heights, and using a moving platform to disengage or engage the bottom weight. Then G is alternated between G_0 and G_{high} for another 10 cycles, with 20 s at G_0 and 10 s at G_{high}. We then move to the next G_{high}, with 11 values of G_{high} tested ranging from 1.65×10^{-3} N to 8.72×10^{-3} N, corresponding to the arrows labeled in Fig. 3(b). The duration was selected to keep the experiment time significantly shorter than the relaxation time.

Following each pressure quench, we calculate the cage order parameters for particle positions, $\boldsymbol{r}_i$, as in previous studies [14,15,24], and for particle orientations, α_i. The first parameter is the characteristic cage size, which is based on the MSD in an individual quench, k, for both positions and orientations,

$$\Delta_r^k(t, t_w) = \frac{1}{\hat{N}} \sum_{i=1}^{\hat{N}} |\boldsymbol{r}_i(t + t_w) - \boldsymbol{r}_i(t_w)|^2,$$

$$\Delta_\alpha^k(t, t_w) = \frac{1}{\hat{N}} \sum_{i=1}^{\hat{N}} [\alpha_i(t + t_w) - \alpha_i(t_w)]^2, \quad (1)$$

where $\hat{N}$ is the number of internal particles. To minimize the effect of possible global deformation, we calculate $\boldsymbol{r}_i$ using the relative position of a particle to the centroid of its Voronoi neighbors [24]. We set the wait time t_w to be 5 s after the quench to P_{high}. Both Δ_r^k and Δ_α^k quickly reach a plateau as particles are caged, and we define $\Delta_r = \langle \Delta_r^k \rangle$ and $\Delta_\alpha = \langle \Delta_\alpha^k \rangle$ as the average of the plateau values over the 10 quenches.

To characterize the cage separation between two quenches, k and k', we calculate

$$\Delta_r^{k,k'}(t) = \frac{1}{\hat{N}} \sum_{i=1}^{\hat{N}} |\boldsymbol{r}_i^k(t) - \boldsymbol{r}_i^{k'}(t)|^2,$$

$$\Delta_\alpha^{k,k'}(t) = \frac{1}{\hat{N}} \sum_{i=1}^{\hat{N}} [\alpha_i^k(t) - \alpha_i^{k'}(t)]^2, \quad (2)$$

using the positions and orientations of the same particle in the two quenches. We define $\Delta_r^{AB} = \overline{\langle \Delta_r^{k,k'} \rangle}$ and $\Delta_\alpha^{AB} = \overline{\langle \Delta_\alpha^{k,k'} \rangle}$ as averages over time (starting from the same t_w) and 45 combination of quenches. The order parameters are normalized by nominal cage sizes, which is σ^2 for position and α_0^2 for orientation with $\alpha_0 = 2\pi/5$.

The results for the two cage order parameters calculated at each quench step are shown in Fig. 4. At low P_{high}, the granular glass is in the stable glass phase where particles can fully explore their cages, resulting in no difference between the cage size Δ_r and the cage separation Δ_r^{AB}. For the orientation order parameters at the first two P_{high} points, Δ_α^{AB} is slightly larger than Δ_α, which is likely the consequence of the global deformation that occurs as the system has not fully reached mechanical equilibrium. Calculating Δ_α^{AB} by only comparing adjacent quench pairs reduces this difference, as shown in the inset to Fig. 4.

As P_{high} increases, the cage size Δ_r and Δ_α decrease. While the cage separations Δ_r^{AB} and Δ_α^{AB} follow the cage sizes at low P_{high}, they reach a plateau starting at $P_{\text{high}}\sigma^2/T_{\text{eff}} \approx 621$ (labeled in Fig. 3), defining the Gardner crossover pressure, $P_G = 0.038$ N/m, with a corresponding density of $\phi_G = 0.437$. This gives $\phi_G/\phi_c \approx 0.99$, similar to the previously reported density ratio [24], and $P_G/P_g \approx 3.13$. For $P_{\text{high}} > P_G$, the difference between the size and the separation widens to larger than an order of magnitude for both position and orientation. This indicates that the granular glass is in a marginal phase, with each
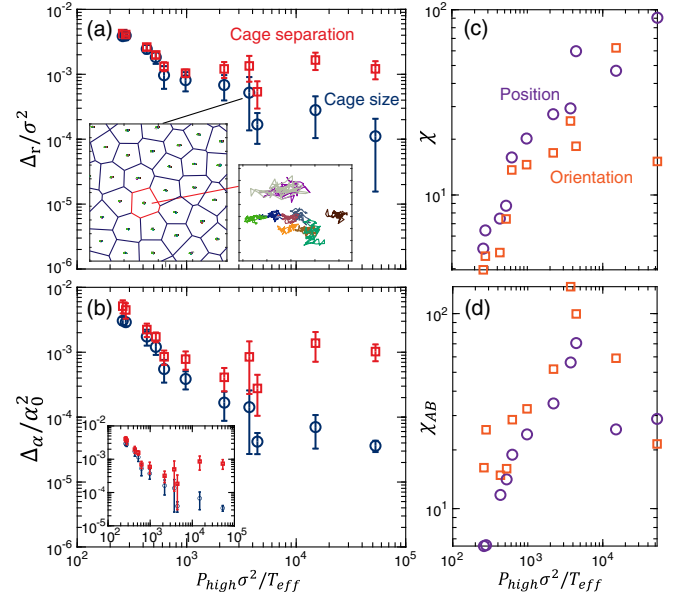

FIG. 4. The transition to the Gardner phase is demonstrated by the onset of a difference between the cage separation Δ^{AB} (red square) and the cage size Δ (blue circle) order parameters with increasing $P_{\text{high}}\sigma^2/T_{\text{eff}}$ for (a) positions and (b) orientations. The inset of (a) shows overlapping particle trajectories in the 10 high pressure cycles along with the Voronoi cells for the initial cycle for $P_{\text{high}}\sigma^2/T_{\text{eff}} = 3732$. The inset of (b) shows the cage order parameters with Δ_α^{AB} calculated only using adjacent cycles. (c) The dynamical susceptibility, χ, and (d) the cage susceptibility, χ_{AB}, for the positions (blue circle) and orientations (orange square) for each pressure.

quench trapping the system in a different sub-basin [1,14,24].

Particles stay caged in each P_{high} step, seen, e.g., in the particle trajectories in the inset of Fig. 4, but at high pressure they are trapped in a subregion of their cages during each quench, as shown by an example of overlaid trajectories of an individual particle. The splitting of Δ and Δ_{AB} is not caused by individual cage-breaking events but by collective behavior of groups of particles. To further demonstrate this, we calculate the dynamical susceptibility [18,24], $\chi = N\langle \text{Var}[\Delta^k(t_w)]\rangle/\Delta^2$, and the cage susceptibility [15,22], $\chi_{AB} = N\overline{\text{Var}[\Delta^{k,k'}(t)]}/\Delta_{AB}^2$, for both particle positions and orientations. Here, χ is calculated using values at different starting times within each quench and averaged over 10 quenches, and χ_{AB} is calculated using values between 45 quench pairs and then averaged over a small time window. The results are shown in Fig. 4, and the susceptibilities for both positions and orientations increase more than an order of magnitude toward the Gardner crossover, indicating increasing correlation in particle dynamics [18,19], and validating a sharp Gardner crossover. Beyond the Gardner crossover, the susceptibilities exhibit nonmonotonic behavior, likely due to dynamical slowing down with increasing pressure [18,19,22].

In summary, the results in this study show significant, unambiguous experimental signals of the Gardner crossover in an active, quasithermal, nearly frictionless granular glass of nonspherically symmetric particles in two spatial dimensions. Although the translational and rotational degrees of freedom have different average energies, they both exhibit signals of the separation of the order parameters and increasing susceptibilities, and the location of the crossover appears to coincide. Our findings underscore the robustness of the Gardner crossover, which was predicted in high dimensional thermal systems with only translational degrees of freedom. Note that the experimental system is relatively small, leading to what appears to be more of a sharp transition than a crossover; system size effects [18,19,22] on marginal stability should be further validated experimentally. In addition, the exploration of sub-basins in the energy landscape in the Gardner regime over longer duration could lead to aging signals such as intermittent increasing of the end-to-end distance. While Gardner physics is expected in low dimensions for hard potentials, the situation for soft potentials, such as those for atomic and molecular glasses, is less clear [39,40], with signatures of marginal stability possibly only observable in large enough, poorly annealed systems. In our gas-fluidized system, particle interactions are not strictly hard-core repulsions because of aerodynamic interactions and slight out-of-plane rotations of the vibrating particles, yet we observe clear signatures of Gardner behavior. It would be interesting to fabricate much softer particles of the same shape to study the influence of interaction potential.

---

*Corresponding author.
djdurian@physics.upenn.edu

[1] L. Berthier and G. Biroli, Theoretical perspective on the glass transition and amorphous materials, Rev. Mod. Phys. **83**, 587 (2011).

[2] P. Charbonneau, J. Kurchan, G. Parisi, P. Urbani, and F. Zamponi, Glass and jamming transitions: From exact results to finite-dimensional descriptions, Annu. Rev. Condens. Matter Phys. **8**, 265 (2017).

[3] E. Gardner, Spin glasses with p-spin interactions, Nucl. Phys. **B257**, 747 (1985).

[4] L. Berthier, G. Biroli, P. Charbonneau, E. I. Corwin, S. Franz, and F. Zamponi, Gardner physics in amorphous solids and beyond, J. Chem. Phys. **151**, 010901 (2019).

[5] H. Yoshino and F. Zamponi, Shear modulus of glasses: Results from the full replica-symmetry-breaking solution, Phys. Rev. E **90**, 022302 (2014).

[6] G. Biroli and P. Urbani, Breakdown of elasticity in amorphous solids, Nat. Phys. **12**, 1130 (2016).

[7] Y. Jin and H. Yoshino, Exploring the complex free-energy landscape of the simplest glass by rheology, Nat. Commun. **8**, 14935 (2017).

[8] D. J. Gross, I. Kanter, and H. Sompolinsky, Mean-Field Theory of the Potts Glass, Phys. Rev. Lett. **55**, 304 (1985).

[9] M. Mézard, G. Parisi, and M. A. Virasoro, *Spin Glass Theory and Beyond: An Introduction to the Replica Method and Its Applications* (World Scientific Publishing Company, Singapore, 1987), Vol. 9.

[10] J. Kurchan, G. Parisi, and F. Zamponi, Exact theory of dense amorphous hard spheres in high dimension I. The free energy, J. Stat. Mech. (2012) P10012.

[11] J. Kurchan, G. Parisi, P. Urbani, and F. Zamponi, Exact theory of dense amorphous hard spheres in high dimension. II. The high density regime and the Gardner transition, J. Phys. Chem. B **117**, 12979 (2013).

[12] P. Charbonneau, J. Kurchan, G. Parisi, P. Urbani, and F. Zamponi, Fractal free energy landscapes in structural glasses, Nat. Commun. **5**, 3725 (2014).

[13] G. Parisi, P. Urbani, and F. Zamponi, *Theory of Simple Glasses: Exact Solutions in Infinite Dimensions* (Cambridge University Press, Cambridge, England, 2020).

[14] P. Charbonneau, Y. Jin, G. Parisi, C. Rainone, B. Seoane, and F. Zamponi, Numerical detection of the Gardner transition in a mean-field glass former, Phys. Rev. E **92**, 012316 (2015).

[15] L. Berthier, P. Charbonneau, Y. Jin, G. Parisi, B. Seoane, and F. Zamponi, Growing timescales and lengthscales characterizing vibrations of amorphous solids, Proc. Natl. Acad. Sci. U.S.A. **113**, 8397 (2016).

[16] C. Scalliet, L. Berthier, and F. Zamponi, Absence of Marginal Stability in a Structural Glass, Phys. Rev. Lett. **119**, 205501 (2017).

[17] C. L. Hicks, M. J. Wheatley, M. J. Godfrey, and M. A. Moore, Gardner Transition in Physical Dimensions, Phys. Rev. Lett. **120**, 225501 (2018).

[18] B. Seoane and F. Zamponi, Spin-glass-like aging in colloidal and granular glasses, Soft Matter **14**, 5222 (2018).

[19] Q. Liao and L. Berthier, Hierarchical Landscape of Hard Disk Glasses, Phys. Rev. X **9**, 011049 (2019).

[20] C. Scalliet, L. Berthier, and F. Zamponi, Nature of excitations and defects in structural glasses, Nat. Commun. **10**, 5102 (2019).

[21] R. C. Dennis and E. I. Corwin, Jamming Energy Landscape is Hierarchical and Ultrametric, Phys. Rev. Lett. **124**, 078002 (2020).

[22] H. Li, Y. Jin, Y. Jiang, and J. Z. Chen, Determining the nonequilibrium criticality of a Gardner transition via a hybrid study of molecular simulations and machine learning, Proc. Natl. Acad. Sci. U.S.A. **118** (2021).

[23] K. Zhang, X. Li, Y. Jin, and Y. Jiang, Machine learning caging order parameters in glasses, arXiv:2111.05573.

[24] A. Seguin and O. Dauchot, Experimental Evidence of the Gardner Phase in a Granular Glass, Phys. Rev. Lett. **117**, 228001 (2016).

[25] K. Geirhos, P. Lunkenheimer, and A. Loidl, Johari-Goldstein Relaxation Far Below t g: Experimental Evidence

for the Gardner Transition in Structural Glasses?, Phys. Rev. Lett. **120,** 085705 (2018).

[26] A. P. Hammond and E. I. Corwin, Experimental observation of the marginal glass phase in a colloidal glass, Proc. Natl. Acad. Sci. U.S.A. **117,** 5714 (2020).

[27] S. Albert, G. Biroli, F. Ladieu, R. Tourbot, and P. Urbani, Searching for the Gardner Transition in Glassy Glycerol, Phys. Rev. Lett. **126,** 028001 (2021).

[28] Y. Wang, J. Shang, Y. Jin, and J. Zhang, Experimental observations of marginal criticality in granular materials, Proc. Natl. Acad. Sci. U.S.A. **119,** e2204879119 (2022).

[29] P. Charbonneau and S. Yaida, Nontrivial Critical Fixed Point for Replica-Symmetry-Breaking Transitions, Phys. Rev. Lett. **118,** 215701 (2017).

[30] I. Ippolito, C. Annic, J. Lemaître, L. Oger, and D. Bideau, Granular temperature: Experimental analysis, Phys. Rev. E **52,** 2072 (1995).

[31] R. Ojha, P.-A. Lemieux, P. Dixon, A. Liu, and D. Durian, Statistical mechanics of a gas-fluidized particle, Nature (London) **427,** 521 (2004).

[32] A. R. Abate and D. J. Durian, Effective Temperatures and Activated Dynamics for a Two-Dimensional Air-Driven Granular System on Two Approaches to Jamming, Phys. Rev. Lett. **101,** 245701 (2008).

[33] L. J. Daniels, T. K. Haxton, N. Xu, A. J. Liu, and D. J. Durian, Temperature-Pressure Scaling for Air-Fluidized Grains Near Jamming, Phys. Rev. Lett. **108,** 138001 (2012).

[34] See Supplemental Material at http://link.aps.org/supplemental/10.1103/PhysRevLett.128.248001 for an example video recording of the experiment.

[35] A. R. Abate and D. J. Durian, Partition of energy for air-fluidized grains, Phys. Rev. E **72,** 031305 (2005).

[36] J. C. Crocker and D. G. Grier, Methods of digital video microscopy for colloidal studies, J. Colloid Interface Sci. **179,** 298 (1996).

[37] S. Farhadi, S. Machaca, J. Aird, B. O. T. Maldonado, S. Davis, P. E. Arratia, and D. J. Durian, Dynamics and thermodynamics of air-driven active spinners, Soft Matter **14,** 5588 (2018).

[38] R. D. Kamien and A. J. Liu, Why is Random Close Packing Reproducible?, Phys. Rev. Lett. **99,** 155501 (2007).

[39] C. Scalliet, L. Berthier, and F. Zamponi, Marginally stable phases in mean-field structural glasses, Phys. Rev. E **99,** 012107 (2019).

[40] B. Shang, P. Guan, and J.-L. Barrat, Elastic avalanches reveal marginal behavior in amorphous solids, Proc. Natl. Acad. Sci. U.S.A. **117,** 86 (2020).